

3.0 TEST MEASUREMENTS

3.1 Overview of Instrumentation

In any experimental program, there are a number of external factors or artifacts of the instrumentation that can influence the data. The goal of this effort was to identify these factors and, to the extent that their influence was significant, adjust the raw data to produce a uniform data set. As part of the posttest analysis effort, ANATECH was also tasked with reviewing the data, identifying significant external influences or artifacts and, if possible, correcting the measurements taken during the LST for these unwanted influences.

A detailed presentation and discussion of the PCCV instrumentation is beyond the scope of this report; a thorough coverage is provided in Ref. 8. This chapter identifies the external influences on the test data and then summarizes the methods to characterize and correct for these influences, if feasible. The details of the corrections are also included in the PCCV test report [8].

The instrumentation measurements in the "data correction" effort, and the effects and phenomena that were addressed, are listed below.

Table 3-1. Instrumentation Measurements

Measurement	Effects Considered for Correction
Displacement	Temperature, Rigid Body Motion
Strains in Special Gaged Rebars	Temperature, Strain Localization
Strains in Liner	Temperature
Pressure	--
Strains in Rebar	Temperature, Strain Localization
Tendon Strains	Temperature
Temperatures	--

3.2 Temperature Effects on Measurements

The data acquisition system was installed and activated more than seven months prior to the LST. Gage measurements taken at various time intervals throughout these seven months provided a vast database of the model's response to changes in ambient temperature. Since the goal of the "data correction" effort is to create a corrected set of data that is free of temperature effects, data were extracted from the database to calibrate correction formulas for each gage. Changes in temperature have a direct influence on the strains and displacements of a free-standing structure. Furthermore, temperature changes have secondary effects on the voltage readouts of strain gages. Both of these effects were considered and quantified in the data correction effort; the former by direct observation of the model response during the calibration periods and the latter by the gage manufacturer. To correct for either phenomena first requires that the temperature be known at every gage, or, in effect, at all possible locations within the PCCV. This information was obtained by developing a temperature mapping algorithm based on interpolation between the matrix of temperature gages. Development of the temperature mapping and data correction algorithms is described in the test report [8].

3.3 Instrumentation Artifacts

In addition to temperature effects, some data artifacts were introduced by the inherent limitations of the instruments themselves or by the methods used to mount them to the structures.

3.3.1 Displacements

While analyses report absolute displacements, that is, in terms of a fixed, global coordinate system, displacement data obtained from experiments are always relative to some other physical structure. In the case of the PCCV model, nearly all the displacements were obtained by measuring the vertical and radial motion of the PCCV relative to the internal instrumentation frame and basemat. The basemat vertical uplift was measured relative to the mudmat. All of these ‘reference’ structures are, themselves, subject to the same influences and loads as the main body of the PCCV model, and therefore also move. A separate set of instruments were applied to these structures to monitor their motion in response to these loads. This data was used to evaluate whether these reference structure motions had a significant influence on the test data. This data is also provided in the test report [8].

With the exception of basemat uplift, the motion of the instrumentation frame to variations in ambient or internal temperature and pressure were negligible relative to the overall motion of the PCCV model, and no corrections were applied to the data.

Regarding the basemat uplift, after the pressure test were completed, it was recognized that the mudmat tended to conform itself to the basemat, and as a result, no relative motion between the basemat and mudmat occurred or was measured. This data was initially interpreted to show that there was no basemat uplift. It was subsequently recognized, therefore, that the vertical displacement transducers on the basemat were not capable of measuring the absolute uplift of the basemat. Unfortunately, no other transducers were available to provide this data and no correction algorithm could be developed. The implications relative to the analysis are described in the next chapter. Fortunately, however, the calculated uplift is relatively small and has very little influence, if any, on the vertical displacement data for the cylinder wall and dome.

3.3.2 Rebar Strains

In addition to the temperature effects described above, there is an additional gage artifact that affects strain gages mounted on deformed rebar. The strain gages used in the PCCV model tests are foil-type resistance gages bonded to the rebar using adhesives. In order to ‘glue’ these gages to the rebar, a relatively flat, smooth surface is required. This surface is obtained by grinding away the local deformations over an area slightly larger than the gage and then polishing this surface. This grinding, while minimized, reduces the cross-sectional area of the rebar at the location where the gage is applied. This locally reduced segment then yields slightly before the rest of the bar, and as a result, strains at the gage location are higher (on the order of 0.5%) than the rest of the bar at stresses just below yield and beyond. This is a significant effect and can be demonstrated analytically for reductions in the cross-sectional area as small as 1%. The phenomena has been illustrated by a series of rebar tensile tests performed at SNL, a few results of which are plotted in Figure 3-1.

This artifact was known from previous experience, and efforts were made to minimize the effect during instrumentation of the rebar. Data was collected on the final bar diameters with the hope that a standardized correction algorithm could be developed.

Recognizing that the rebar gage measurements tend to overpredict the corresponding engineering strain, especially in the range of initial yield (i.e. between $\epsilon = 0.002$ and $\epsilon = 0.015$), one possible correction algorithm was developed, as follows. Based on measurements of the instrumented rebar, the typical area reduction as a result of the grinding is 2%. It is assumed that for all strain ϵ , there is a unique stress, σ , according to the engineering stress-versus engineering strain data. Using the averaged data for the SD390-D13 bars, the yield curve is approximately

ϵ	σ
.002	58 ksi
.009	60.9 ksi
.013	62.06 ksi
.015	63.075 ksi
.020	66.7 ksi

For a measured local rebar strain, ϵ_i , the corresponding stress, σ_i , is "looked-up" from the stress-strain data for the bar in question.

The nominal stress in the bar, i.e. outside the locally reduced area, is $\sigma_n = \sigma_i / (\text{Area Ratio})$.

The nominal strain, ϵ_n , is then returned from the yield function.

This correction is also illustrated in Figure 3-2. Unfortunately, this correction did not account for the complete gage effect. Attempts to apply the correction to all the rebar data did not improve the data, and in some cases made it worse. As a result, it was decided not to apply the correction to the data, but to recognize its presence and consider it, as appropriate, when comparing the data to analyses.

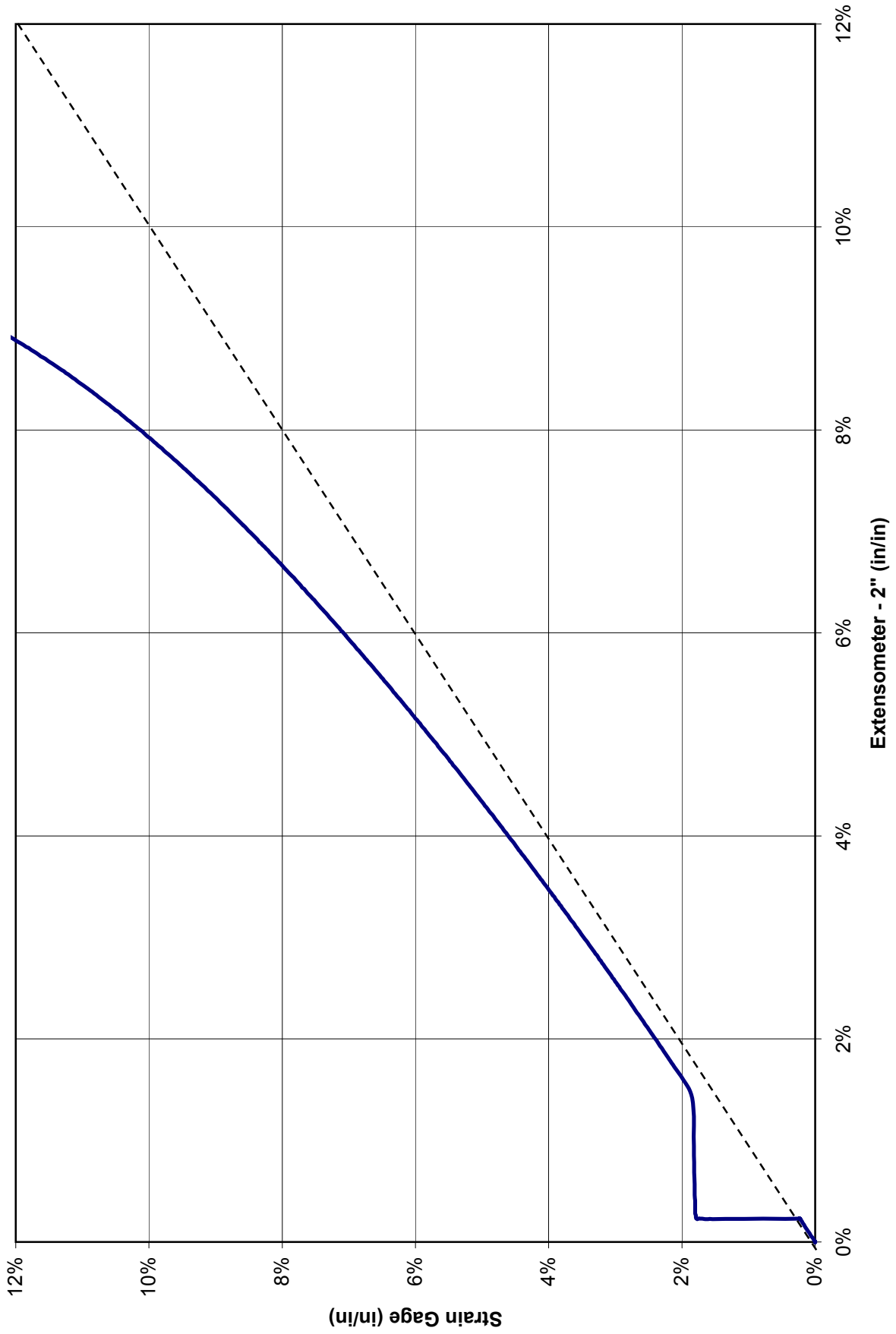


Figure 3-1. Comparison of Strain at Z6 (Azimuth 135 degrees, Elev. 6280)

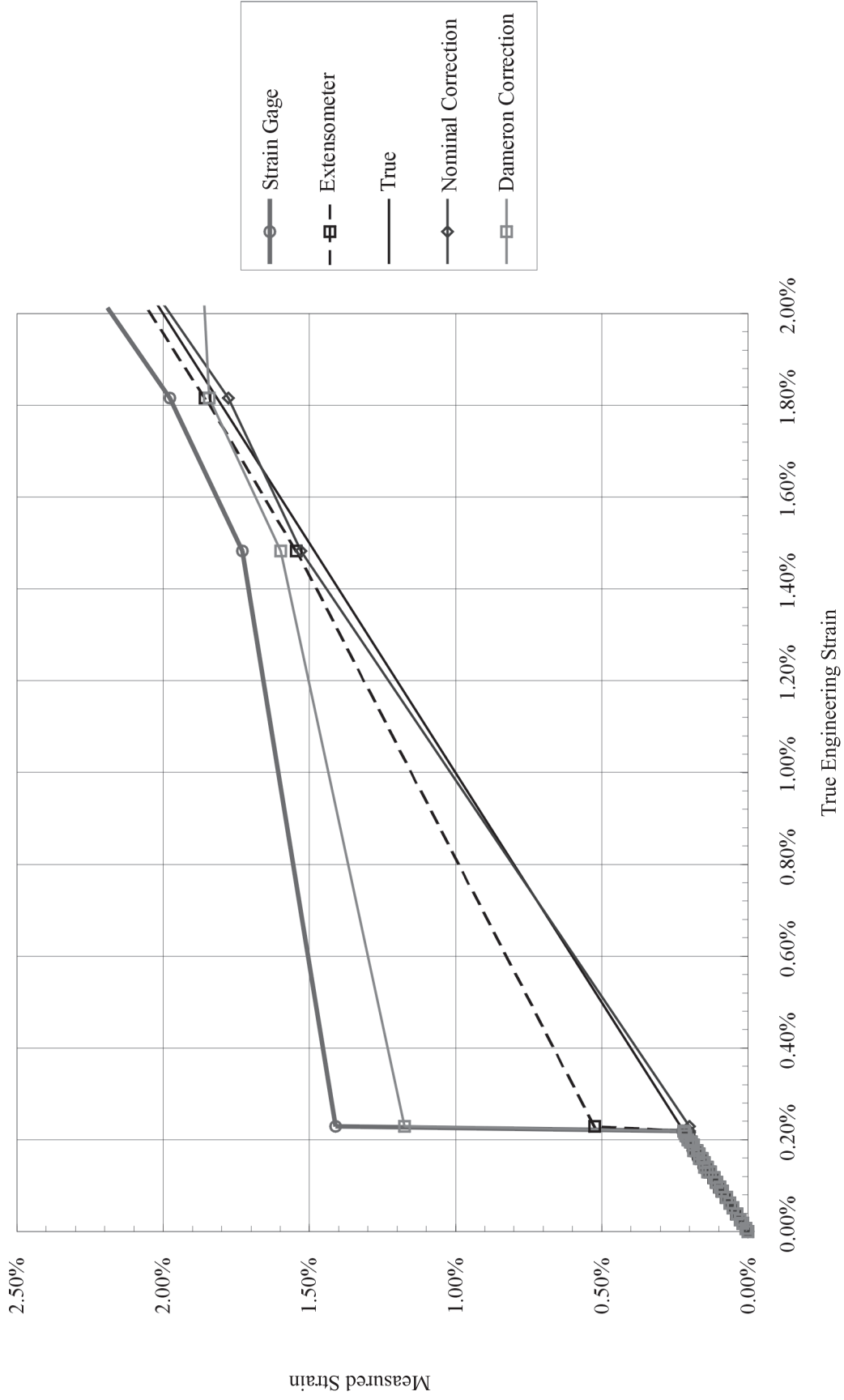


Figure 3-2. Rebar Tensile Test Simulation

4.0 COMPARISONS OF PRETEST ANALYSIS RESULTS WITH THE TEST

The pretest analyses consisted of global axisymmetric analysis and local model analysis. The local models analyzed were: the E/H region, the personnel airlock region, and the M/S penetration region. A detailed 3DCM was also developed to investigate tendon behavior in the cylinder and 3D effects that drive the local strain concentrations near the penetrations. A highly detailed representation of the wall-basemat juncture region was included in the 2D axisymmetric model, making a total of five pretest analysis models. The results of the initial pretest analyses were published in 1999 [1] and were the basis of the SNL/ANATECH contribution to an international Round Robin Pretest Analysis exercise [3]. As described in Chapter 2, a final pretest analysis was completed in 2000, immediately prior to the LST.

This chapter compares the test measurements to both pretest analyses. Test data are compared to the results of the analysis. For example, the results of the 3DCM model, with its explicit tendon representation, are compared to the tendon strain or force data, whereas results of the axisymmetric model are compared to those response data that are relatively independent of the azimuth, such as free-field displacements and the behavior of the wall-base junction and the dome response. The same rationale is used to compare and discuss failure modes.

A set of 55 SOLs, each associated with an actual gage (or set of gages), was identified by the project team to provide a comprehensive suite of data sets for comparison to the round robin analysis results. The SOLs are described in Table 4-1, along with the associated gage(s). After reviewing the PCCV LST data, these locations were indeed useful comparison points. This chapter thus makes extensive use of comparisons at these 55 SOLs. In some cases, to learn more about how the analysis or the test responded at another location, additional plots and comparisons were extracted from the analytical models and the test data.

Table 4-1. Standard Output Locations

Loc. #	Type	Orientation	Az. (deg)	El. (m)	Comments	General Location	Instr. ID (1st)	ID (2nd gage)
1	Displacement	Vertical	135	0	Outside Cylinder	Top of Basemat	DL-M-Z0-01	
2	Displacement	Radial	135	0.25	Inside Liner Surface	Base of Cylinder	DL-R-Z2-01	
3	Displacement	Radial	135	1.43	Inside Liner Surface	Base of Cylinder	DL-R-Z3-01	
4	Displacement	Radial	135	2.63	Inside Liner Surface	Base of Cylinder	DT-R-Z4-01	
5	Displacement	Radial	135	4.68	Inside Liner Surface	E/H elev.	DT-R-Z5-01	
6	Displacement	Radial	135	6.2	Inside Liner Surface	Approximate Midheight	DT-R-Z6-01	
7	Displacement	Radial	135	10.75	Inside Liner Surface	Springline	DT-R-Z9-01	
8	Displacement	Vertical	135	10.75	Inside Liner Surface	Springline	DT-M-Z9-01	
9	Displacement	Horiz. (Rad)	135	14.55	Inside Liner Surface	Dome 45 deg	CP-R-Z11-01	
10	Displacement	Vertical	135	14.55	Inside Liner Surface	Dome 45 deg.	DT-M-Z11-01	
11	Displacement	Vertical	135	16.13	Inside Liner Surface	Dome apex	DT-M-Z13-01	
12	Displacement	Radial	90	6.2	Inside Liner Surface	Midheight @ Buttress	CP-R-D6-01	
13	Displacement	Radial	90	10.75	Inside Liner Surface	Springline @ Buttress	CP-R-D9-01	

Table 4-1. Standard Output Locations

Loc. #	Type	Orientation	Az. (deg)	El. (m)	Comments	General Location	Instr. ID (1st)	ID (2nd gage)
14	Displacement	Radial	324	4.675	Inside Liner Surface	Center of E//H	CP-R-L5-01	
15	Displacement	Radial	62	4.525	Inside Liner Surface	Center of A/L	CP-R-C5-01	
16	Rebar Strain	Meridional	135	0.05	Inner Rebar Layer	Base of Cylinder	RS-M-Z1-01	
17	Rebar Strain	Meridional	135	0.05	Outer Rebar Layer	Base of Cylinder	RS-M-Z1-02	
18	Rebar Strain	Meridional	135	0.25	Inner Rebar Layer	Base of Cylinder	RS-M-Z2-01	
19	Rebar Strain	Meridional	135	0.25	Outer Rebar Layer	Base of Cylinder	RS-M-Z2-02	
20	Rebar Strain	Meridional	135	1.43	Inner Rebar Layer	Base of Cylinder	RS-M-Z3-01	
21	Rebar Strain	Meridional	135	1.43	Outer Rebar Layer	Base of Cylinder	RS-M-Z3-02	
22	Rebar Strain	Hoop	135	6.2	Outer Rebar Layer	Midheight	RS-C-Z6-02	
23	Rebar Strain	Meridional	135	6.2	Outer Rebar Layer	Midheight	RS-M-Z6-02	
24	Rebar Strain	Hoop	135	10.75	Outer Rebar Layer	Springline	RS-C-Z9-02	
25	Rebar Strain	Meridional	135	10.75	Inner Rebar Layer	Springline	RS-M-Z9-01	RS-M-Z9-03
26	Rebar Strain	Meridional	135	10.75	Outer Rebar Layer	Springline	RS-M-Z9-02	RS-M-Z9-04
27	Rebar Strain	Hoop	135	14.55	Outer Rebar Layer	Dome 45 deg.	RS-C-Z11-02	
28	Rebar Strain	Meridional	135	14.55	Inner Rebar Layer	Dome 45 deg.	RS-M-Z11-01	RS-M-Z11-03
29	Rebar Strain	Meridional	135	14.55	Outer Rebar Layer	Dome 45 deg.	RS-M-Z11-02	RS-M-Z11-04
30	Rebar Strain	Meridional	90	0.05	Inner Rebar Layer	Base of Cylinder @ Buttress	RS-M-D1-01	
31	Rebar Strain	Meridional	90	0.05	Outer Rebar Layer	Base of Cylinder @ Buttress	RS-M-D1-02	
32	Rebar Strain	Hoop	90	6.2	Outer Rebar Layer	Midheight @ Buttress	RS-C-D6-02	
33	Rebar Strain	Meridional	90	6.2	Outer Rebar Layer	Midheight @ Buttress	RS-M-D6-02	
34	Liner Strain	Meridional	0	0.01	Inside Liner Surface	Base of Cylinder	LSI-M-A1-01	
35	Liner Strain	Meridional	0	0.01	Outside Liner Surface	Base of Cylinder	LSO-M-A1-03	
36	Liner Strain	Meridional	135	0.25	Inside Liner Surface	Base of Cylinder	LSI-M-Z2-01	

Table 4-1. Standard Output Locations

Loc. #	Type	Orientation	Az. (deg)	El. (m)	Comments	General Location	Instr. ID (1st)	ID (2nd gage)
37	Liner Strain	Hoop	135	0.25	Inside Liner Surface	Base of Cylinder	LSI-C-Z2-01	
38	Liner Strain	Meridional	135	6.2	Inside Liner Surface	Midheight	LSI-M-Z6-01	
39	Liner Strain	Hoop	135	6.2	Inside Liner Surface	Midheight	LSI-C-Z6-01	
40	Liner Strain	Meridional	135	10.75	Inside Liner Surface	Springline	LSI-M-Z9-01	
41	Liner Strain	Hoop	135	10.75	Inside Liner Surface	Springline	LCI-C-Z9-01	
42	Liner Strain	Meridional	135	16.13	Inside Liner Surface	Dome apex	LSI-M-Z13-01	LSI-C-Z13-01
43	Liner Strain	Meridional	90	6.2	Inside Liner Surface	Midheight @ Buttress	LSI-M-D6-01	
44	Liner Strain	Hoop	90	6.2	Inside Liner Surface	Midheight @ Buttress	LSI-C-D6-01	
45	Liner Strain	Hoop	334	4.675	Inside Liner Surface	10 mm from thickened plate	LSI-C-A5-03	
46	Liner Strain	Hoop	58	4.525	Inside Liner Surface	10 mm from thickened plate	LSI-C-C5-03	
47	Base Liner	Radial	135	0	100 mm Inside Cylinder	FF Basemat Liner Strain	LSI-R-Z1-08	
48	Tendon Strain	Hairpin	180	15.6	Tendon - V37	Tendon Apex	TT-M-G12-01	TF-M-G12-01
49	Tendon Strain	Hairpin	135	10.75	Tendon - V46	Tendon Springline	TT-M-Z9-01	TF-M-Z9-01
50	Tendon Strain	Hoop	90	6.58	Tendon - H53	Mid. Tendon	TT-C-D6-01	TT-C-D6-02
51	Tendon Strain	Hoop	180	6.58	Tendon - H53	¼ - Tendon	TT-C-G6-01	TF-C-G6-01
52	Tendon Strain	Hoop	280	6.58	Tendon - H53	Tendon Near Buttress	TT-C-K6-01	TF-C-K6-01
53	Tendon Strain	Hoop	0	4.57	Tendon - H35	Tendon between E/H and A/L	TT-C-A5-01	TT-C-A5-02
54	Tendon Force	Hairpin	241	-1.16	Tendon - V37	Tendon Gallery	TL—10-03	
55	Tendon Force	Hoop	275	6.58	Tendon - H53	@ Buttress	TL-C-J6-02	